

OPEN

Defects, Dopants and Sodium Mobility in Na_2MnSiO_4

Navaratnarajah Kuganathan[1] & Alexander Chroneos[1,2]

Received: 21 June 2018
Accepted: 12 September 2018
Published online: 02 October 2018

Sodium manganese orthosilicate, Na_2MnSiO_4, is a promising positive electrode material in rechargeable sodium ion batteries. Atomistic scale simulations are used to study the defects, doping behaviour and sodium migration paths in Na_2MnSiO_4. The most favourable intrinsic defect type is the cation anti-site (0.44 eV/defect), in which, Na and Mn exchange their positions. The second most favourable defect energy process is found to be the Na Frenkel (1.60 eV/defect) indicating that Na diffusion is assisted by the formation of Na vacancies via the vacancy mechanism. Long range sodium paths via vacancy mechanism were constructed and it is confirmed that the lowest activation energy (0.81 eV) migration path is three dimensional with zig-zag pattern. Subvalent doping by Al on the Si site is energetically favourable suggesting that this defect engineering stratergy to increase the Na content in Na_2MnSiO_4 warrants experimental verification.

Sodium ion batteries have attracted attention as a dominant power source in large scale energy storage applications due to the low cost and high abundance of sodium as compared to lithium[1–3].

New class of cathode materials providing large quantity of Na ions in sodium batteries can lead to the high power density and high energy density. Several promising sodium based cathode materials such as $NaFePO_4$[4–6], Na_2FePO_4F[7,8], $Na_3V_2(PO_4)_3$[9,10] and Na_xTMO_2 (TM = Ti, V, Cr, Mn, Fe, Co and Ni)[11–13] were reported in the experimental studies. Discovery of novel cathode materials is still active to produce high capacity battery to satisfy the growing demand.

Orthosilicate Na_2MnSiO_4 has been recently proposed as a promising Na storage material because of its impressive sodium storage performance, low cost and environmentally benign[14–19]. The structural stability of this material is mainly provided by the $(SiO_4)^{4-}$ matrix via strong Si-O bonds. Further, it may be possible to extract more than one sodium more readily from Na_2MnSiO_4 since Mn can form the Mn^{4+} oxidation state. Chen *et al.*[15] synthesized Na_2MnSiO_4 by a sol-gel method and reported a reversible capacity of 125 $mAhg^{-1}$ at a rate of C/10 using an ionic liquid electrolyte at elevated temperatures. Law *et al.*[14] prepared Na_2MnSiO_4 *via* a modified two-step route and reported an impressive sodium storage performance of 210 $mAhg^{-1}$ at 0.1 C. Using first-principles calculations, Zhang *et al.*[19] investigated ion diffusion mechanism of Na_2MnSiO_4 and concluded that the Na ion diffusion is faster than Li ion diffusion in Li_2MnSiO_4. There are a limited number of experimental and theoretical work reported in the literature.

As experiments cannot provide detailed information about the defects and Na ion diffusion paths with activation energies, classical modelling techniques are widely used to calculate those properties. This theoretical approach has been successfully applied on a wide range of lithium ion battery materials and a few sodium ion battery materials[20–25]. Very recently, we have applied this simulation technique to examine the defect chemistry, lithium transport and the effect of dopants on lithium vacancy formation on the Li_5FeO_4[26], Li_2CuO_2[27] and $Li_9V_3(P_2O_7)_3(PO_4)$[28]. The present study uses atomistic modeling techniques to calculate the energetics for the formation of defects, solution of trivalent dopants and Na ion diffusion paths in Na_2MnSiO_4.

Results and Discussion

Na_2MnSiO_4 structure. The crystal structure of Na_2MnSiO_4 exhibits a monoclinic crystallographic structure with space group *Pn* (lattice parameters a = 7.02857 Å, b = 5.60957 Å, c = 5.33391 Å, $\alpha = 90.0°$, $\beta = 89.7949°$ and $\gamma = 90°$) as reported by Nalbandyan *et al.*[16] In the Fig. 1, crystal structure of Na_2MnSiO_4 is shown together with bonding nature of all cations forming corner-sharing tetrahedral units with four O atoms. First, experimental monoclinic crystal structure was reproduced using classical pair potentials as tabulated in Table S1 in the

[1]Department of Materials, Imperial College London, London, SW7 2AZ, United Kingdom. [2]Faculty of Engineering, Environment and Computing, Coventry University, Priory Street, Coventry, CV1 5FB, United Kingdom. Correspondence and requests for materials should be addressed to N.K. (email: n.kuganathan@imperial.ac.uk) or A.C. (email: alexander.chroneos@imperial.ac.uk)

Parameter	Calc	Expt[13]	|Δ| (%)
a (Å)	6.995595	7.028570	0.47
b (Å)	5.644977	5.609570	0.63
c (Å)	5.334769	5.333910	0.02
α (°)	90.0000	90.0000	0.00
β (°)	89.7683	89.7949	0.03
γ (°)	90.0000	90.0000	0.00

Table 1. Calculated and Experimental Structural Parameters for Monoclinic (P*n*) Na_2MnSiO_4.

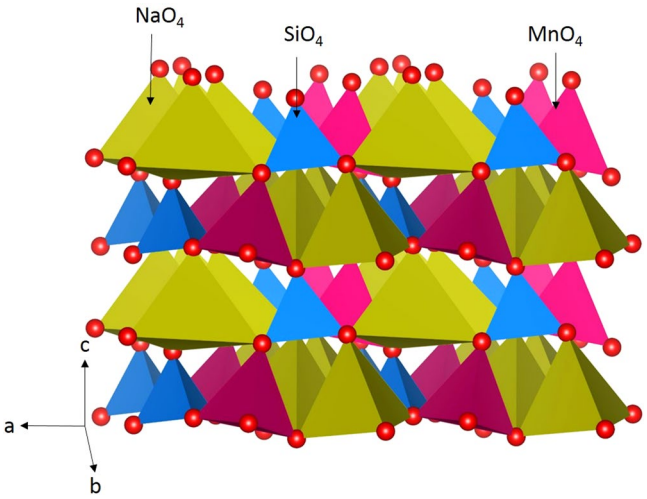


Figure 1. Crystal structure of Na_2MnSiO_4 (space group P*n*).

Supplementary Information. There is an excellent agreement between experimental and calculated equilibrium-lattice constants (refer to Table 1).

Intrinsic defect processes. Next we calculated different isolated point defects including vacancies and interstitials to calculate the Frenkel and Schottky-type defect formation energies in Na_2MnSiO_4. These intrinsic defect energetics can provide useful information about the electrochemical behavior of Na_2MnSiO_4. Here we write equations for the Frenkel, Schottky and anti-site defect formation using the Kröger-Vink notation[29].

$$\text{Na Frenkel: } Na_{Na}^{X} \rightarrow V_{Na}^{'} + Na_{i}^{\bullet} \tag{1}$$

$$\text{Mn Frenkel: } Mn_{Mn}^{X} \rightarrow V_{Mn}^{''} + Mn_{i}^{\bullet\bullet} \tag{2}$$

$$\text{O Frenkel: } O_{O}^{X} \rightarrow V_{O}^{\bullet\bullet} + O_{i}^{''} \tag{3}$$

$$\text{Si Frenkel: } Si_{Si}^{X} \rightarrow V_{Si}^{''''} + Si_{i}^{\bullet\bullet\bullet\bullet} \tag{4}$$

$$\text{Schottky: } 2\,Na_{Na}^{X} + Mn_{Mn}^{X} + Si_{Si}^{X} + 4\,O_{O}^{X} \rightarrow 2\,V_{Na}^{'} + V_{Mn}^{''} + V_{Si}^{''''} + 4V_{O}^{\bullet\bullet} + Na_2MnSiO_4 \tag{5}$$

$$Na_2O \text{ Schottky: } 2\,Na_{Na}^{X} + O_{O}^{X} \rightarrow 2\,V_{Na}^{'} + V_{O}^{\bullet\bullet} + Na_2O \tag{6}$$

$$MnO \text{ Schottky: } Mn_{Mn}^{X} + O_{O}^{X} \rightarrow V_{Mn}^{''} + V_{O}^{\bullet\bullet} + MnO \tag{7}$$

$$SiO_2 \text{ Schottky: } Si_{Si}^{X} + 2\,O_{O}^{X} \rightarrow V_{Si}^{''''} + 2\,V_{O}^{\bullet\bullet} + SiO_2 \tag{8}$$

$$\text{Na/Mn antisite (isolated): } Na_{Na}^{X} + Mn_{Mn}^{X} \rightarrow Na_{Mn}^{'} + Mn_{Na}^{\bullet} \tag{9}$$

Migration path	Na-Na separation (Å)	Activation energy (eV)
A	3.2687	0.77
B	3.3041	0.81
C	3.4568	0.98
D	3.2250	0.63

Table 2. Calculated Na-Na separations and activation energies for the sodium ion migration between two adjacent Na sites refer to Fig. 3.

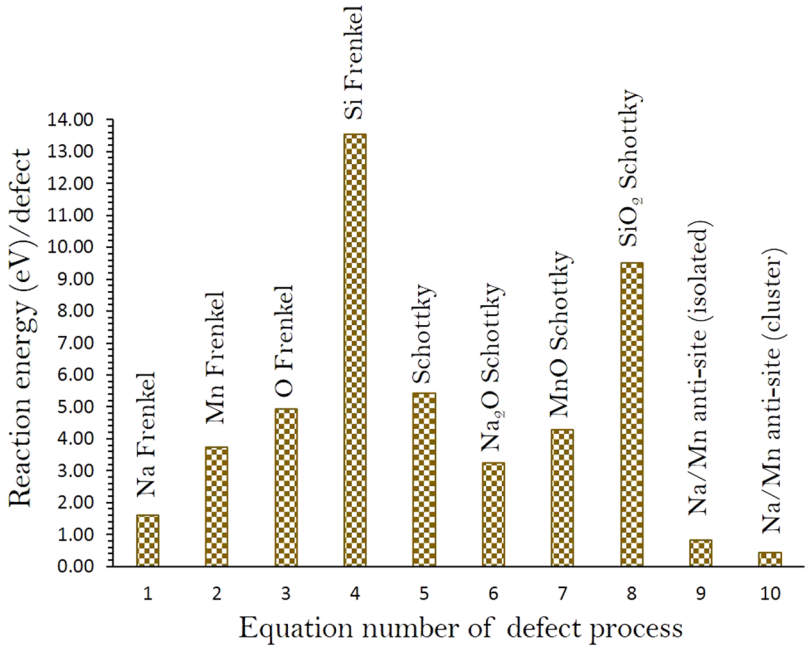


Figure 2. Energetics of intrinsic defect process in monoclinic Na_2MnSiO_4.

$$\text{Na/Mn antisite (cluster): } Na_{Na}^{X} + Mn_{Mn}^{X} \rightarrow \{Na_{Mn}^{'}: Mn_{Na}^{\bullet}\}^{X} \tag{10}$$

Figure 2 shows the reaction energies for these intrinsic defect processes (refer to Table S2 for the energies). Na-Mn anti-site was calculated to be the most favorable intrinsic disorder meaning that at high temperatures a small percentage of Na on Mn sites ($Na_{Mn}^{'}$) and Mn on Na sites ($Mn_{Na}^{\bullet}$) will be observed. In the relaxed defect structure, a small amount of distortion is observed in the cation-oxygen bond lengths and bond angles, but overall structure of the lattice was not distorted significantly. This type of defect has been observed experimentally in different class of Li ion cathode battery materials during cycling and theoretically in some as prepared Na ion cathode materials[23–25,30–35]. The Na Frenkel was found to be the second most favourable defect process. The Frenkel and Schottky defect energies were calculated to be highly endothermic meaning that they are unfavorable. The formation enthalpy of Na_2O Schottky (relation 6) is 3.25 eV per defect (refer to Table S2, Supplementary Information). At elevated temperatures, this process can take place to form further $V_{Na}^{'}$ and $V_{O}^{\bullet\bullet}$.

Sodium ion-diffusion. The intrinsic sodium ion diffusion of Na_2MnSiO_4 is discussed in this section. Activation energy of Na ion diffusion together with diffusion paths are important when Na_2MnSiO_4 is assessed as a potential material in sodium ion batteries. The current computaional technique enables the calculation of Na diffusion paths together with activation energies, which are diffcult to investigate by experiments. For the Na vacancy migration, four Na local hops (A, B, C and D) were identified. Hop A is between two Na sites with the jump distance of 3.2687 Å and the migration energy is calculated to be 0.77 eV (refer to Table 2). The migration path for hop A is in the *ac* plane and Na ion moves via a curved trajectory. In the hop B, Na ions diffuses in the *ac* plane with a curved trajectory but the jump distance of 3.3041 Å and migration energy of 0.81 eV which are different from those calculated for hop A. Hops C and D are in the *ab* plane with each forming curve trajectories. Their jump distances are 3.4568 Å and 3.3350 Å with corresponding migration energies of 0.98 eV and 0.63 eV respectively. Two possible three dimensional lower energy long range paths (A → B → A → B) and (C → D → C → D) connecting local Na hops were identified as shown in Fig. 3. These two paths exhibited zig-zag pattern with overall activation energies of 0.81 eV and 0.98 eV respectively. We considered other possible long range paths connecting local Na hops. However, the lowest overall activation energy was calculated to be 0.81 eV. Figure 4 reports the energy profile diagrams for Na local hops with activation energies. Zhang *et al.*[19] calculated the ion diffusion mechanism in Li_2MnSiO_4 and Na_2MnSiO_4 using density functional theory and concluded that Na^+ migration has relatively lower

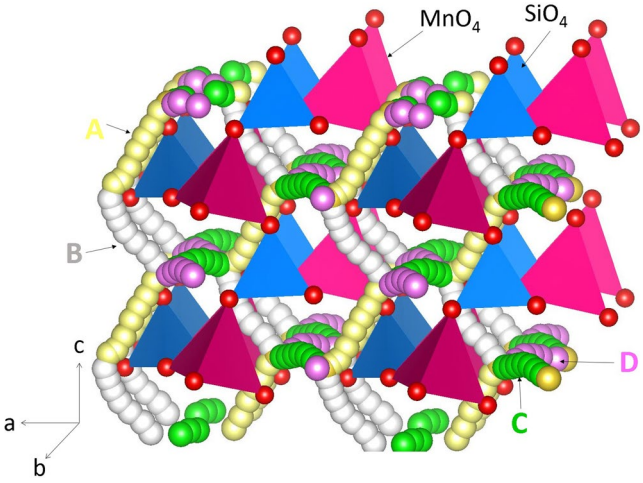


Figure 3. Possible long range sodium vacancy migration paths considered. Local Na migration paths are shown in green, yellow, white and purple atoms. SiO_4 and MnO_4 tetrahedral units are shown blue and pink colors respectively.

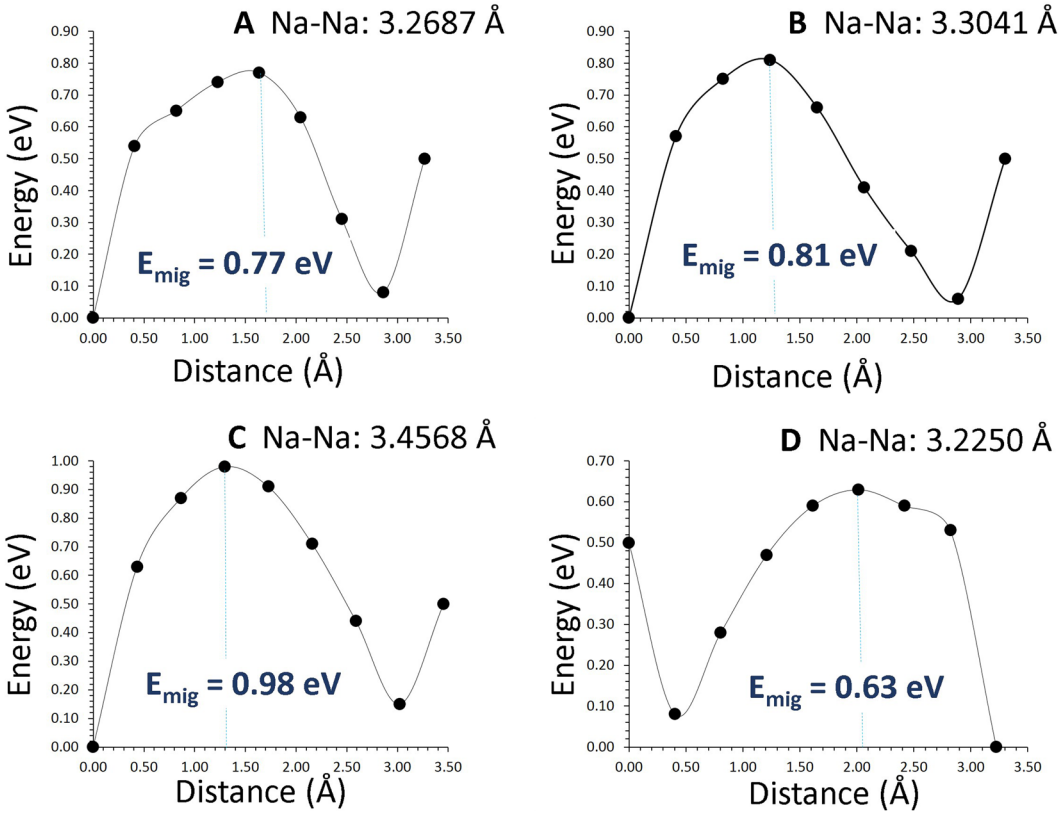


Figure 4. Four different energy profiles [as shown in Fig. 3] of Na vacancy hopping between two adjacent Na sites in Na_2MnSiO_4.

activation energy barrier than that of Li^+ migration. In our previous modelling for monoclinic Li_2MnSiO_4, the lowest over all activation energy for Li ion migration is 1.58 eV[21]. In the current study, the lowest overall Na ion migration barrier is calculated to be 0.81 eV much lower than that found for Li ion migration in agreement with the study of Zhang *et al.*[19]. Furthermore, in their study, Na^+ ion migrate *via* three dimensional channels and the overall activation energy is calculated to be 0.54 eV. The activation energy difference is due to two different methodologies. Also density functional theory (DFT) is constrained by finite size effects. Small system sizes are a well-known source of error in DFT calculations. Furthermore, in the present study, ions were treated as fully charged as point defects in a highly ionic material might be expected to be in their fully ionic charge states. The position of the highest potential energy along the migration path is defined as the activation energy of migration.

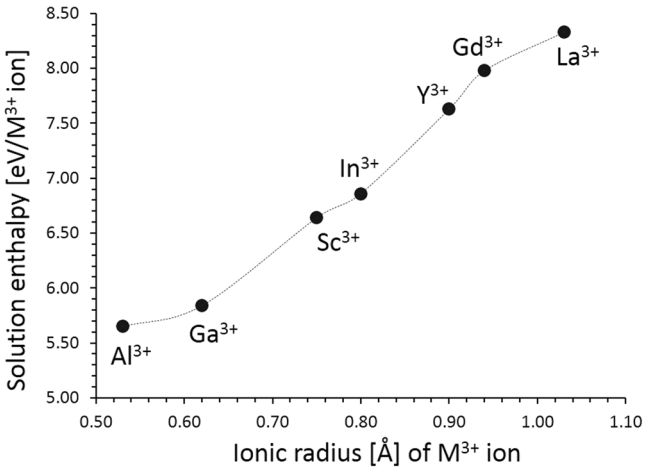


Figure 5. Enthalpy of solution of R_2O_3 (R = Al, Ga, Sc, In, Y, Gd and La) with respect to the R^{3+} ionic radius in Na_2MnSiO_4.

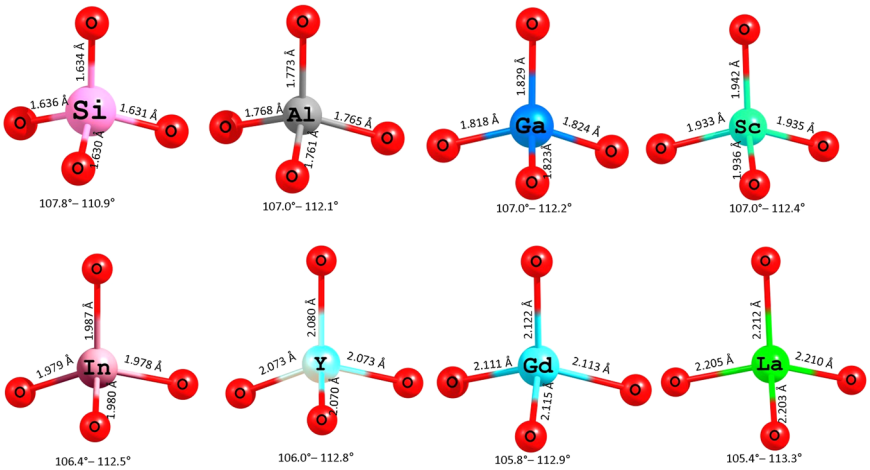


Figure 6. Tetrahedral SiO_4 unit in the relaxed structure of undoped Na_2MnSiO_4 and the coordination formed by the dopants on the Si site with neighbour oxygen.

Trivalent doping. Incorporation of additional sodium into the as-prepared material will enhance the capacity and further increase the applicability of Na_2MnSiO_4 as a potential cathode material for sodium ion batteries. A possible approach to incorporate additional Na is by doping trivalent cations on Si site through creating Na interstitials. Similar approach has been previously demonstrated in Li_2MnSiO_4 cathode material[21]. Here we considered the solution of R_2O_3 (R = Al, Ga, Sc, In, Y, Gd and La) via the following process (in Kröger-Vink notation):

$$R_2O_3 + 2\,Si_{Si}^{X} + Na_2O \rightarrow 2\,R_{Si}^{'} + 2\,Na_i^{\bullet} + 2\,SiO_2 \quad (11)$$

We report the solution energies of R_2O_3 in Fig. 5. Our calculation reveals that the most favorable dopant solution energy is found for Al^{3+}. This suggests that a possible synthesis-doping strategy of introducing additional sodium into Na_2MnSiO_4, although the exact amount of Al incorporation cannot be predicted. The possible composition of Al-doped Na_2MnSiO_4 would be $Na_{2+x}MnSi_{1-x}Al_xO_4$ (x = 0.0–1.0). The second most favorable dopant is Ga^{3+}. The solution energy increases further with the dopant size.

Figure 6 shows the dopants forming tetrahedral units with adjacent oxygen atoms together with dopant-oxygen bond lengths and oxygen-dopant-oxygen bond angles. For comparison, the tetrahedral SiO_4 unit in the relaxed structure of defect free Na_2MnSiO_4. The ionic radii of Si^{4+} and Al^{3+} in tetrahedral coordination are 0.26 Å and 0.39 Å respectively. The ionic radius of Al^{3+} is 0.13 Å larger than that of Si^{4+}. In the SiO_4 unit, all four Si-O bonds (~1.630 Å) are equal. In AlO_4 unit, Al-O bond lengths (~1.760 Å) and bond angles are slightly larger than that found in SiO_4 unit and smaller than that found in other RO_4 (R = Ga, Sc, In, Y, Gd and La) units. This is reflected in the lowest solution energy for Al. The ionic radius of Ga^{3+} is 0.47 Å slightly larger (by 0.09 Å) than that that of Al^{3+}. There is a slight increase in the Ga-O bond lengths and bond angles. This is reflected in the second lowest solution enthalpy. From Sc^{3+} to La^{3+}, solution enthalpy steadily increases with ionic radius reflecting in

the bond lengths and bond angles. Highly endothermic solution energy values indicate that they will not occur at low temperatures. At elevated temperatures, this process would become feasible.

Summary. In conclusion, the atomistic simulation techniques were employed to calculate intrinsic defects, sodium ion diffusion paths and trivalent doping in order to assess Na_2MnSiO_4 as a promising sodium battery cathode. The dominant energy defect process is Na-Mn anti-site defect suggesting that there would be small intrinsic concentration of Mn on Na sites at operating temperatures. The long range Na ion diffusion path with lowest migration energy was calculated to be three dimensional with the migration energy of 0.81 eV. Solution energies of R_2O_3 (R = Al, Ga, Sc, In, Y, Gd and La) were calculated to increase extra Na ions in Na_2MnSiO_4. Our calculation suggests that doping Al^{3+} on Si site is an efficient strategy to increase the Na content in Na_2MnSiO_4 requiring experimental investigation.

Computational methods. In the present study we have used the classical pair potential methodology using the GULP package[36]. In essence this is based on the Born model for ionic crystals. The interionic interactions are long-range (attractive: Coulombic) and short-range (repulsive: electron-electron repulsion). For the latter we employed well established Buckingham potentials (Table S1, Supplementary Information)[21,23,37–41]. The relaxation of the atomic positions and lattice parameters was achieved by employing the Broyden-Fletcher-Goldfarb-Shanno (BFGS) algorithm[42]. For the lattice relaxation round defects the Mott-Littleton method[43] (inner spherical region larger than 700 ions) immediately. Na was placed and fixed at 7 interstitial positions in a linear route between two vacancy sites (all other ions were allowed to relax). Using this series of calculations the maximum energy corresponds to the activation energy of migration along the route. Here we have employed the full charge ionic model with the calculations in the dilute limit. These are sufficient and will correctly calculate trends in energies, however, defect energies are bound to be overestimated[44,45].

References

1. Ellis, B. L. & Nazar, L. F. Sodium and sodium-ion energy storage batteries. *Curr. Opin. Solid State Mater. Sci.* **16**, 168–177 (2012).
2. Yabuuchi, N., Kubota, K., Dahbi, M. & Komaba, S. Research Development on Sodium-Ion Batteries. *Chem. Rev* **114**, 11636–11682 (2014).
3. Palomares, V., Casas-Cabanas, M., Castillo-Martinez, E., Han, M. H. & Rojo, T. Update on Na-based battery materials. A growing research path. *Energy Environ. Sci.* **6**, 2312–2337 (2013).
4. Oh, S.-M., Myung, S.-T., Hassoun, J., Scrosati, B. & Sun, Y.-K. Reversible $NaFePO_4$ electrode for sodium secondary batteries. *Electrochem. Commun* **22**, 149–152 (2012).
5. Fang, Y. *et al*. High-Performance Olivine $NaFePO_4$ Microsphere Cathode Synthesized by Aqueous Electrochemical Displacement Method for Sodium Ion Batteries. *ACS Appl. Mater. Interfaces* **7**, 17977–17984 (2015).
6. Tang, W. *et al*. High-performance $NaFePO_4$ formed by aqueous ion-exchange and its mechanism for advanced sodium ion batteries. *J. Mater. Chem. A* **4**, 4882–489 (2016).
7. Kawabe, Y. *et al*. Synthesis and electrode performance of carbon coated Na2FePO4F for rechargeable Na batteries. *Electrochem. Commun.* **13**, 1225–1228 (2011).
8. Kosova, N. V., Podugolnikov, V. R., Devyatkina, E. T. & Slobodyuk, A. B. Structure and electrochemistry of $NaFePO_4$ and Na_2FePO_4F cathode materials prepared via mechanochemical route. *Mater. Res. Bull* **60**, 849–857 (2014).
9. Jian, Z. *et al*. Carbon coated $Na_3V_2(PO_4)_3$ as novel electrode material for sodium ion batteries. *Electrochem. Commun* **14**, 86–89 (2012).
10. Jiang, X. *et al*. Extending the cycle life of $Na_3V_2(PO_4)_3$ cathodes in sodium-ion batteries through interdigitated carbon scaffolding. *J. Mater. Chem. A* **4**, 14669–14674 (2016).
11. Han, M. H., Gonzalo, E., Singh, G. & Rojo, T. A Comprehensive review of sodium layered oxides: Powerful cathodes for Na-ion batteries. *Energy Environ. Sci.* **8**, 81–102 (2015).
12. Guo, S. *et al*. Cation-mixing stabilized layered oxide cathodes for sodium-ion batteries. *Sci. Bull.* **63**, 376–384 (2018).
13. Sun, Y., Guo, S. & Zhou, H. Adverse effects of interlayer-gliding in layered transition-metal oxides on electrochemical sodium-ion storage. *Energy Environ. Sci* (2018).
14. Law, M., Ramar, V. & Balaya, P. Na_2MnSiO_4 as an attractive high capacity cathode material for sodium-ion battery. *J. Power Sources* **359**, 277–284 (2017).
15. Chen, C.-Y., Matsumoto, K., Nohira, T. & Hagiwara, R. Na_2MnSiO_4 as a positive electrode material for sodium secondary batteries using an ionic liquid electrolyte. *Electrochem. Commun.* **45**, 63–66 (2014).
16. Nalbandyan, V. B. *et al*. A_2MnXO_4 Family (A = Li, Na, Ag; X = Si, Ge): Structural and Magnetic Properties. *Inorg. Chem.* **56**, 14023–14039 (2017).
17. Xia, N. *et al*. Electrochemical performances of Na_2MnSiO_4 as an energy storage material in sodium-ion capacitors. *J. Appl. Electrochem.* **47**, 343–349 (2017).
18. Zhu, H., Wang, J., Liu, X. & Zhu, X. Facile preparation of a Na_2MnSiO_4/C/graphene composite as a high performance cathode for sodium ion batteries. *RSC Adv* **7**, 14145–14151 (2017).
19. Zhang, P. *et al*. Ion diffusion mechanism in Pn $Na_xLi_{2-x}MnSiO_4$. *Cryst Eng Comm* **17**, 2123–2128 (2015).
20. Islam, M. S., Driscoll, D. J., Fisher, C. A. J. & Slater, P. R. Atomic-scale investigation of defects, dopants, and lithium transport in the $LiFePO_4$ olivine-type battery material. *Chem. Mater.* **17**, 5085–5092 (2005).
21. Kuganathan, N. & Islam, M. S. Li_2MnSiO_4 Lithium Battery Material: Atomic-Scale Study of Defects, Lithium Mobility, and Trivalent Dopants. *Chem. Mater.* **21**, 5196–5202 (2009).
22. Fisher, C. A. J., Kuganathan, N. & Islam, M. S. Defect chemistry and lithium-ion migration in polymorphs of the cathode material Li_2MnSiO_4. *J. Mater. Chem. A* **1**, 4207–4214 (2013).
23. Treacher, J. C., Wood, S. M., Islam, M. S. & Kendrick, E. Na_2CoSiO_4 as a cathode material for sodium-ion batteries: structure, electrochemistry and diffusion pathways. *Phys. Chem. Chem. Phys* **18**, 32744–32752 (2016).
24. Wood, S. M., Eames, C., Kendrick, E. & Islam, M. S. Sodium Ion Diffusion and Voltage Trends in Phosphates $Na_4M_3(PO_4)_2P_2O_7$ (M = Fe, Mn, Co, Ni) for Possible High-Rate Cathodes. *J. Phys. Chem. C* **119**, 15935–15941 (2015).
25. Clark, J. M., Barpanda, P., Yamada, A. & Islam, M. S. Sodium-ion battery cathodes $Na_2FeP_2O_7$ and $Na_2MnP_2O_7$: diffusion behaviour for high rate performance. *J. Mater. Chem. A* **2**, 11807–11812 (2014).
26. Kuganathan, N., Iyngaran, P. & Chroneos, A. Lithium diffusion in Li_5FeO_4. *Sci. Rep.* **8**, 5832 (2018).
27. Kordatos, A., Kuganathan, N., Kelaidis, N., Iyngaran, P. & Chroneos, A. Defects and lithium migration in Li_2CuO_2. *Sci. Rep* **8**, 6754 (2018).

28. Kuganathan, N., Ganeshalingam, S. & Chroneos, A. Defects, Dopants and Lithium Mobility in $Li_9V_3(P_2O_{7)3}(PO_4)_2$. *Sci. Rep.* **8**, 8140 (2018).
29. Kröger, F. A. & Vink, H. J. In *Solid State Physics* Vol. 3 (eds Frederick Seitz & David Turnbull) 307–435 (Academic Press, 1956).
30. Nyten, A., Kamali, S., Haggstrom, L., Gustafsson, T. & Thomas, J. O. The lithium extraction/insertion mechanism in Li_2FeSiO_4. *J. Mater. Chem.* **16**, 2266–2272 (2006).
31. Ensling, D., Stjerndahl, M., Nyten, A., Gustafsson, T. & Thomas, J. O. A comparative XPS surface study of Li_2FeSiO_4/C cycled with LiTFSI- and LiPF6-based electrolytes. *J. Mater. Chem.* **19**, 82–88 (2009).
32. Liu, H. *et al*. Effects of Antisite Defects on Li Diffusion in $LiFePO_4$ Revealed by Li Isotope Exchange. *J. Phys. Chem C* **121**, 12025–12036 (2017).
33. Kempaiah Devaraju, M., Duc Truong, Q., Hyodo, H., Sasaki, Y. & Honma, I. Synthesis, characterization and observation of antisite defects in $LiNiPO_4$ nanomaterials. *Sci. Rep.* **5**, 11041 (2015).
34. Armstrong, A. R., Kuganathan, N., Islam, M. S. & Bruce, P. G. Structure and lithium transport pathways in Li_2FeSiO_4 Cathodes for Lithium Batteries. *J. Am. Chem. Soc.* **133**, 13031–13035 (2011).
35. Politaev, V. V., Petrenko, A. A., Nalbandyan, V. B., Medvedev, B. S. & Shvetsova, E. S. Crystal structure, phase relations and electrochemical properties of monoclinic Li_2MnSiO_4. *J. Solid State Chem.* **180**, 1045–1050 (2007).
36. Gale, J. D. & Rohl, A. L. The General Utility Lattice Program (GULP). *Molec. Simul.* **29**, 291–341 (2003).
37. Grimes, R. W. Solution of MgO, CaO and TiO_2 in a-Al_2O_3. *J. Am. Ceram. Soc.* **77**, 378–384 (1994).
38. Grimes, R. W. *et al*. The effects of ion size on solution mechanism and defect cluster geometry. *Ber. Bunden-Ges. Phys. Chem.* **101**, 1204–1210 (1997).
39. McCoy, M. A., Grimes, R. W. & Lee, W. E. Planar intergrowth structures in the ZnO–In_2O_3 System. *Philos. Mag. A* **76**, 1187–1201 (1997).
40. Busker, G., Chroneos, A., Grimes, R. W. & Chen, I.-W. Solution mechanisms for dopant oxides in yttria. *J. Am. Ceram. Soc.* **82**, 1553–1559 (1999).
41. Tabira, Y., Withers, R. L., Minervini, L. & Grimes, R. W. Systematic structural change in selected rare earth oxide pyrochlores as determined by wide-angle CBED and a comparison with the results of atomistic computer simulation. *J. Solid State Chem.* **153**, 16–25 (2000).
42. Gale, J. D. GULP: A computer program for the symmetry-adapted simulation of solids. *J. Chem. Soc. Faraday Trans.* **93**, 629–637 (1997).
43. Mott, N. F. & Littleton, M. J. Conduction in polar crystals. I. Electrolytic conduction in solid salts. *Trans. Faraday Soc.* **34**, 485–499 (1938).
44. Rushton, M. J. D. & Chroneos, A. Impact of uniaxial strain and doping on oxygen diffusion in CeO_2. *Sci. Rep* **4**, 6068 (2014).
45. Jay, E. E., Rushton, M. J. D., Chroneos, A., Grimes, R. W. & Kilner, J. A. Genetics of superionic conductivity in lithium lanthanum titanates. *Phys. Chem. Chem. Phys.* **17**, 178–183 (2015).

Acknowledgements

Computational facilities and support were provided by High Performance Computing Centre at Imperial College London.

Author Contributions

N.K. performed the calculations. All the authors analyzed and discussed the results and contributed to the writing of the paper.

Additional Information

Supplementary information accompanies this paper at https://doi.org/10.1038/s41598-018-32856-7.

Competing Interests: The authors declare no competing interests.

Publisher's note: Springer Nature remains neutral with regard to jurisdictional claims in published maps and institutional affiliations.

Open Access This article is licensed under a Creative Commons Attribution 4.0 International License, which permits use, sharing, adaptation, distribution and reproduction in any medium or format, as long as you give appropriate credit to the original author(s) and the source, provide a link to the Creative Commons license, and indicate if changes were made. The images or other third party material in this article are included in the article's Creative Commons license, unless indicated otherwise in a credit line to the material. If material is not included in the article's Creative Commons license and your intended use is not permitted by statutory regulation or exceeds the permitted use, you will need to obtain permission directly from the copyright holder. To view a copy of this license, visit http://creativecommons.org/licenses/by/4.0/.

© The Author(s) 2018